3-21-2019

Cooperative Transport in a Multi-Particle, Multi-Dimensional Flashing Ratchet

Ofer Kedem

Emily A. Weiss

Journal of Physical Chemistry C, Vol. 123, No. 11 (March 21, 2019): 6913-6921. DOI.

Cooperative Transport in a Multi-Particle, Multi-Dimensional Flashing Ratchet

Ofer Kedem
Center for Bio-Inspired Energy Science, Northwestern University, Chicago, Illinois
Department of Chemistry, Northwestern University, Evanston, Illinois
Emily A. Weiss
Center for Bio-Inspired Energy Science, Northwestern University, Chicago, Illinois
Department of Chemistry, Northwestern University, Evanston, Illinois

Abstract

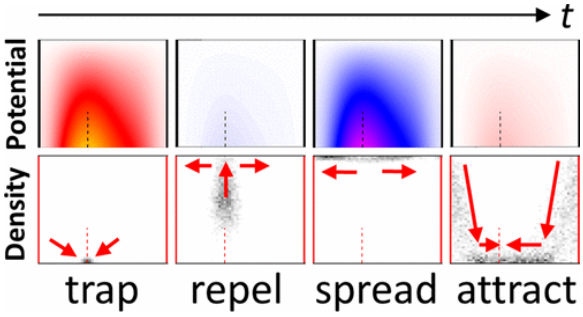

Random and undirected forces are rectified in biological and synthetic systems using ratcheting mechanisms, which employ periodic asymmetric potentials and nonequilibrium conditions to produce useful transport. The density of motors or transported particles is known to strongly affect the nature and efficacy of transport in biological systems, as well as in synthetic ratchets and active swimmer systems. While experimental ratchet implementations typically employ potentials varying in two dimensions (2D), the role of the density of interacting particles in such a system has not been modeled. Prompted by experimental observations and building upon previous simulations, this paper describes the ratcheting process of interacting particles in a 2D flashing ratchet, studied using classical simulations. Increased particle density is found to allow effective ratcheting at higher driving frequencies, compared to the low-density or non-interacting case. High densities also produce a new ratcheting mode at low driving frequencies, based on independent trajectories of high kinetic-energy particles, more than doubling transport at low frequencies.

Introduction

Molecular motors in biological systems utilize local asymmetries to rectify isotropic forces, such as chemical energy and Brownian motion.(1−3) Their mechanism, known as “ratcheting”, is fundamentally different from transport in response to the application of an overall potential gradient and can even do work against such a gradient.(4) Ratcheting relies on breaking temporal symmetry and spatial inversion symmetry in the direction of transport, and it requires the constant input of energy into the system. In biological systems, spatial asymmetry stems from the structure of the motors and their binding and conformational transitions, and temporal asymmetry results from cycles of consumption of chemical fuel (adenosine triphosphate (ATP)) and heavy damping of the motion.(5,6) In synthetic implementations, specifically of the “flashing ratchet” type, the amplitude of a periodic potential with asymmetric repeating units is oscillated in time, thus providing both asymmetry and energy input.(7) This potential is typically electrical and is used to drive electrically charged particles, from electrons(8,9) to charged molecules(10) to nano- or microspheres.(11) The ratchet mechanism displays properties characteristic of a highly out-of-equilibrium process, including an extreme sensitivity to all operating conditions: small variations in parameters such as the shape of the ratchet potential, frequency of driving, and the density of ratcheted particles change the magnitude and sometimes even the direction of transport.(1,12−14) Biological motors can exhibit cooperative transport, traffic jam formation and avoidance, self-assembled density patterns, and far-from-equilibrium transport phase transitions.(15−17) The precise nature of the interaction between the motors strongly affects their ability to work cooperatively, as was shown in theoretical work.(18)

We have previously established the classical nature of transport within a damped electron ratchet(19) and, accordingly, were able to clarify several mechanisms of transport in our experimental electron ratchets with classical simulations of a charged particle ratchet. Specifically, we showed that introducing a second dimension (the thickness of the transport layer)—through which the particles travel and the applied field permeates—enables a previously unknown mechanism of symmetry breaking and, consequently, the ability to produce

ratchet current with a time-unbiased driving function, such as a sine wave.(20) That work explained our ability to drive an experimental flashing electron ratchet with a sine wave potential.(21,22) A major experimental result, fundamental to the ratchet mechanism, however, remained mysterious: a direct correlation of the optimal frequency of the ratchet—the oscillation frequency of the potential that produces the peak short-circuit current—with the carrier density. This result points to the critical role of interparticle interactions in the operation of the ratchet and mandates interpretation through multidimensional, multiparticle simulations.

Several previous theoretical studies reveal a strong dependence of ratchet behavior on the density of repelling particles, specifically, single(23−25) or multipeaked(14,26) (including reversals of current polarity) dependence of ratchet current on particle density. Additionally, Nitzan and co-workers explored the ratcheting of interacting particles on a discrete-site chain and identified at least one regime where ratchet efficiency increases with increasing density of repulsive particles.(27) Even without considering interparticle interaction, a particle ensemble can behave differently from a single particle—in a feedback-controlled ratchet, an increasing particle count was shown to reduce the effectiveness of the feedback protocol and made periodic (nonfeedback) switching more effective at high densities.(28) Interparticle interactions can be utilized to create the asymmetric gradients required for ratcheting by pinning some of the interacting particles in a specific pattern, as was shown theoretically.(29,30) Excluded volume interactions in a magnetic colloidal ratchet have been shown experimentally to cause quantization of the transport as a function of field strength, due to the formation of particle clusters of defined sizes.(31)

In one case of soft-core colloids interacting in a two-dimensional (2D) plane and subject to a one-dimensional (1D) on/off asymmetric potential,(25) the optimal frequency of the ratchet was also found to vary with the particle density; however, the authors varied the spatial periodicity of the potential along with the density, so the application of these results to the experimentally relevant case—where the particle density changes, but the periodicity of the potential is fixed—is not straightforward. No study has explored the role of interparticle interactions in a ratchet with a 2D potential similar to the common experimental case, periodic and asymmetric in one dimension (the direction of transport), and aperiodic and nonuniform in the perpendicular dimension, nor explained the microscopic processes resulting in changes in current or optimal frequency in multiparticle systems, even for 1D systems. In the molecular machines field, recent results indicate that an uneven allocation of free energy across the duration of a cycle maximizes the current produced, highlighting the importance of exploring in detail the individual steps involved in the ratcheting process.(32)

Here, we model a classical, sine wave-driven, 2D flashing particle ratchet, with a range of particle densities resulting in interparticle Coulombic repulsion, explore its behavior at different particle densities and operating frequencies, and elucidate the mechanisms responsible for the observed effects. The configuration of the modeled system is based on our experimental studies and is similar to other common experimental realizations; it thus allows for direct comparisons with previous work and can guide future experimental implementations of flashing particle and electron ratchets. We report two main observations: (i) increasing particle density enables transport at higher frequencies, as the interparticle repulsion serves as an additional driving force to spread particles in the potential wells; and (ii) at high particle densities and low driving frequencies, some particles obtain enough energy from interparticle collisions to escape the potential wells, when most particles are trapped, and explore the asymmetric potential landscape, traversing multiple spatial periods. The latter effect more than doubles the overall transport velocity.

Computational Details

We conduct finite-element simulations of an ensemble of interacting particles in a box of height *d* and length *l*, with periodic boundary conditions in the *x*-direction, and diffusely reflecting top and bottom boundaries; the center of the box is defined as $(x = 0, z = 0)$. Experimental ratchet systems are typically uniform in the y-

direction, so we only model the $x - z$ plane. The particles are governed by a Newton–Langevin equation, eq 1, where m is the mass of a particle:

$$m\ddot{r}(t) = -\frac{dV(t,\mathbf{r})}{d\mathbf{r}} - \gamma\dot{\mathbf{r}} + F_B + F_{C,i} + \xi(t) \quad (1)$$

$V(t,\boldsymbol{r}) = g(t)U(\boldsymbol{r})$ is the spatially and temporally varying potential; $\gamma = 6\pi\mu r_{\mathrm{p}}$ is the viscous drag coefficient, where μ is the dynamic viscosity of the medium, and r_{p} is the radius of a particle; F_{B} describes collisions with boundaries; $\mathrm{F}_{\mathrm{C},i}$ is the Coulombic interparticle interaction; and $\xi(t)$ is a white noise term.

The potential $U(\mathbf{r})$ is periodic in x with period L, such that $U(x) = U(x + L)$. An asymmetric periodic potential $U(x, z = -d/2)$ is applied to the bottom boundary of the simulation box, eq 2

$$U(x, z = -d/2) = \frac{1}{2}\alpha_1\left(1 + \sin\left(\frac{2\pi x}{L}\right)\right) - \frac{1}{2}\alpha_2\left(1 + \sin\left(\frac{4\pi x}{L}\right)\right)\ \alpha_1 = 1;\ \alpha_2 = 0.25 \quad (2)$$

while the top boundary is grounded, $U(x,\ z = d/2) = 0$. The potential applied from the bottom thus decays toward the top, according to the dielectric properties of the medium, creating the two-dimensional potential landscape $U(\mathbf{r})$. The temporal waveform $g(t)$ is defined by eq 3, where A is the amplitude of the applied potential, and f is the frequency of oscillation.

$$g(t) = A \cdot \sin(2\pi f t) \quad (3)$$

The potential for one spatial period, at four time-steps during the temporal oscillation, is plotted in Figure 1a; the potential and the positions of particles are recorded at 200 time-steps during each oscillation, regardless of the oscillation frequency. F_{B} describes diffuse scattering from the bottom and top boundaries of the simulation box, defined as $w_{\mathrm{b}}(x) = -d/2;\ w_{\mathrm{t}}(x) = d/2$. The velocity immediately following a boundary scattering event is defined by eq 4, where $\theta = acos\Gamma = \frac{\pi}{2}$, Γ is a uniformly distributed random number in the range from −1 to 1, and $\hat{t}$ and $\hat{n}$ are unit vectors tangential and normal to the boundary, respectively.

$$v(t + dt) = |v(t)|\sin\theta\hat{t} + |v(t)|\cos\theta\hat{n}$$

(4)

$\xi(t)$ is a δ-correlated Gaussian white noise term, simulating the Brownian force, such that $\langle\xi(t)\rangle = 0$, and $\langle\xi(t)\xi(s)\rangle = 2\gamma k_{\mathrm{B}}T\delta(t - s)$, where k_{B} is the Boltzmann constant, and T is the temperature of the system,(33) in accordance with the dissipation–fluctuation theorem. $\mathrm{F}_{\mathrm{C},i}$, defined by eq 5, represents the force acting on the ith particle due to Coulombic repulsion by any other particles within 1000 nm of the particle under consideration; particles farther apart are assumed not to interact.

$$F_{\mathrm{C},i} = \frac{e^2}{4\pi\varepsilon_0}\sum_{j=1}^{N}\frac{(r_i - r_j)}{|r_i - r_j|^3}$$

(5)

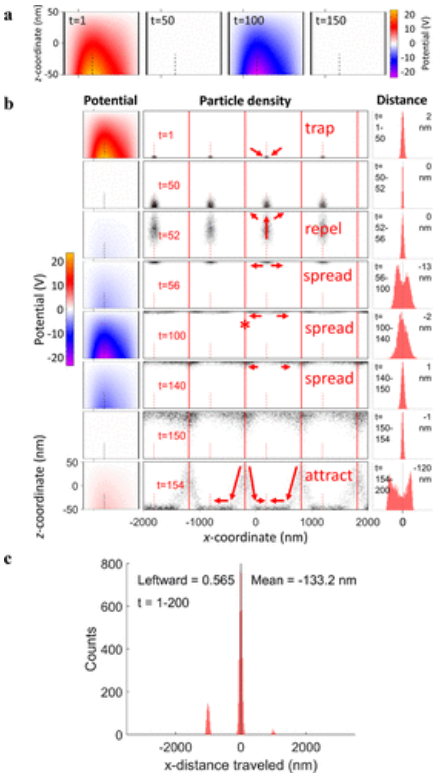

Figure 1. (**a**) Electric potential map in one spatial period at four equally spaced time-steps during the oscillation (indicated step t of 200 per oscillation). (**b**) The ratcheting process broken into eight time steps during a single oscillation. (**left**) Electric potential map in one spatial period; (**center**) density of non-interacting particles within our four-period simulation box (the color scale is normalized for each panel separately; darker shade indicates higher particle density); dashed and solid vertical lines indicate the positions of the absolute maxima and minima of the applied potential, respectively; (**right**) histograms of the distances traveled by individual particles in the *x*-direction between the step pictured in the density map and the next step. The histograms all span 2500 nm on the *x*-axis, and their *y*-scales vary. The mean travel distance of the ensemble is listed on the plot, in nanometers. (**c**) Histogram of the distances traveled during an entire oscillation. The plots in (b, c) incorporate the results from all analyzed oscillations and replicates at $f = 5$ kHz.

In eq 5, *e* is the elementary charge, ε_0 is the permittivity of vacuum, and r_i and r_j are the position vectors of the ith and jth particles, respectively (all particles carry a single negative charge).

The spatial periodicity of the potential in the *x*-direction is $L = 1$ μm, and we simulate a box of four periods ($l = 4L$), with periodic boundary conditions in the *x*-direction. The medium is water, with a dynamic viscosity at room temperature μ(293 K) = 0.001 009 Pa·s and relative dielectric constant $\varepsilon_r = 80$. The viscosity depends on the temperature, as detailed in the Supporting Information section. The particles have a radius of $r_p = 2.5$ nm, which determines the degree of drag and the particle mass, but the model does not include any non-Coulombic interaction (e.g., hard-sphere; collisions with the boundaries are specified by the center of a particle); the density of Au (19.3 g/cm^3); and carry a charge of −*e* each, where *e* is the elementary charge. At the start of the simulation, particles are released from randomly chosen points spread over the simulation area. In every simulation, we propagate the system during 10–20 oscillations of the potential, meaning the actual duration of the simulation varies with the frequency *f*. The number of oscillations is chosen to be long enough to allow the system to settle into a dynamic equilibrium, erasing the effect of initial particle positions. When analyzing results, we ignore the current during an initial number of oscillations (2 of 10, or 10 of 20) to allow the system to settle into a dynamic steady state (the period we analyze is termed the “analyzed oscillations” henceforth). We

repeat every set of conditions four (for most cases) or eight (for eight particles per box) times and report the mean of the ensemble velocity.

The system is simulated at $T = 293.15$ K, unless otherwise noted. The values of the parameters used in the simulation are listed in Table S1 in the Supporting Information. The simulations were performed using the finite-element software COMSOL Multiphysics 5.3a-5.4. The time steps taken by the solver are determined by the generalized-α method,(34) but the duration of each step cannot exceed $(2000f)^{-1}$.

Results and Discussion

A Detailed Look at the 2D Ratchet Mechanism for Non-Interacting Particles

The potential is applied from the bottom boundary of the transport layer, and it oscillates in time as a sine wave between attractive and repulsive stages (positive and negative polarities, respectively). Figure 1b shows the electrostatic maps (left) and the spatial distributions (center) of *non-interacting* particles at eight time-steps during a single temporal period of the oscillation of the potential at a frequency of $f = 5$ kHz. The positions of particles are sampled at 200 time-steps per temporal oscillation (regardless of the frequency), and we highlight specific steps or periods of interest. This figure also shows histograms (right) of the distances traveled by all particles in the ensemble between these time-steps. The behavior at this frequency is representative of the general mechanism for non-interacting particles at all frequencies. During the oscillation, the particles (i) *trap* at the bottom boundary due to the attractive field; (ii) *repel* to the top boundary due to the repulsive field; (iii) *spread* along the top boundary due to repulsion from the applied potential and diffusion, to reach the points of weakest repulsion; and (iv) *attract* back to the bottom boundary.

During the *spread* stage ($t = 100$ of 200), the particles reach the barrier between two spatial periods (solid line, marked with asterisk). This milestone is critical for ratcheting, as only particles to have crossed this barrier can be attracted to the adjacent potential well on the left when the potential turns attractive again, rather than return to their starting well. The histograms on the right-hand-side of Figure 1b show the distances traveled in the *x*-direction (Δx) by individual particles between one time-step and the next and list the mean ensemble Δx. Using the histograms, we see that ratchet current, defined as net travel of the ensemble in the *x*-direction without an applied bias in that direction, mostly occurs during the *attract* stage, while the *trap*, *repel*, and *spread* stages show largely symmetric movement of particles and small net transport.

To summarize the mechanism of current production—the repulsive (negative) potential sends particles to the top boundary, where a fraction of them cross the barrier between adjacent potential wells. The asymmetry of the repulsive potential causes the majority of particles to be located to the left of the barrier at the end of the *spread* phase, such that, when the potential turns attractive, more particles move left (to the next potential well), than return to their original well. Particles then travel along the bottom boundary and come to rest at the bottoms of the potential wells. At every oscillation of the potential, a plurality of particles return to their original wells (central peak in Figure 1c), and smaller fractions move one spatial period to the left and right, respectively. The asymmetry between the left and right peaks in the histogram for the entire oscillation (Figure 1c) reflects the transport achieved by the ratcheting process during that oscillation. Though this general mechanism is operative for a range of driving frequencies, as the frequency increases, the process becomes less efficient. The *spread* stage must last long enough for the particles to reach the barrier between spatial periods, and as the time allotted for this stage decreases, fewer particles reach the barrier.

The Magnitude and Frequency Dependence of the Ratchet Current Vary with Particle Density

The behavior of the ratchet (with respect to particle trajectories, frequency dependence, sign, and magnitude of the net particle velocity) does not, of course, depend on particle density if the particles are non-interacting (the case labeled “1” in Figure 2); simulating an ensemble of non-interacting particles is equivalent to multiple single-particle simulations. If we introduce a Coulombic repulsion between particles, as described in the Computational Details section above, we see clear trends in ratchet behavior on going from low densities (as few as eight particles per simulation box) to high densities (up to 512 particles per simulation box). For instance, for 8–32 particles, the ratchet operates optimally at an ∼10 kHz oscillation frequency (Figure 2a). With increasing particle density, the optimal operating frequency (“peak frequency”) increases, as does the peak velocity. Figure 2b shows the velocity versus particle density for three oscillation frequencies. Tracking mean particle velocity as a function of oscillation frequency (as we do in Figure 2a) is analogous to the experimental measurement of short-circuit current while scanning oscillation frequency. It is not, however, a proper view with which to analyze the effect of particle density on transport mechanism, because, even if the fraction of the particles that switch to an adjacent potential well during an oscillation period remains unchanged from density to density, increasing the oscillation frequency will trivially increase the observed velocity by giving the particles more chances to jump wells. We therefore plot (in Figure 2c,d) the mean distance traveled by the ensemble *per oscillation*, calculated by dividing the velocity on the *y*-axis of Figure 2a by the oscillation frequency; this parameter is analogous to an experimental measurement of the power conversion efficiency of the ratchet. Figure 2c,d contains the same data, but Figure 2c highlights the dependence of transport on particle density for densities of 1–256 particles per box, while Figure 2d highlights this dependence for densities of 64–512 particles per box. We use two separate figures to emphasize that the dependence of transport on particle density appears to separate into two distinct responses. The velocity and distance per oscillation plots are plotted with standard deviations of the mean in Figure S4 of the Supporting Information.

Figure 2

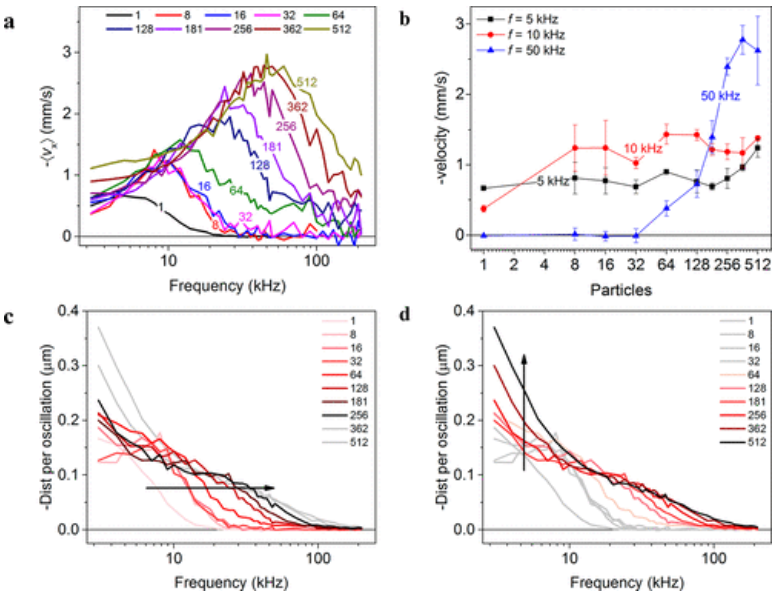

Figure 2. (**a**) Mean ensemble time-averaged negative velocity as a function of oscillation frequency, for different particle numbers (indicated). (**b**) Mean ensemble time-averaged negative velocity as a function of particle count per simulation box, for three oscillation frequencies (indicated); (**c**, **d**) the data in (a), divided by frequency, to give the distance traveled by the ensemble per oscillation, and separated into two plots to highlight the two density regimes. Simulations are run at intervals of 1 kHz between 3 and 10 kHz, 2 kHz between 12 and 50 kHz,

and 10 kHz above. The plotted values in all panels are the means of four replicates (or eight replicates for eight particles, to increase signal-to-noise ratio), and in (b) the error bars are standard deviation of the mean.

Figure 2c shows that, for particle densities from 1 to 16 per box, we observe net transport from −0.10 to −0.15 µm per oscillation (corresponding to a net 10–15% of particles moving one well to the left) at low frequencies and a turn-off of transport at frequencies above 20 kHz. For 16 to 256 particles, the frequency response broadens, such that, at 256 particles, transport occurs up to ∼100 kHz, allowing use of higher driving frequencies to ratchet. Figure 2d shows that, between 256 and 512 particles, the high-frequency region of the response stabilizes, but transport at low frequencies (∼3–10 kHz) increases to values greater than −0.35 µm per oscillation, equivalent to 35% of particles moving one well to the left.

Below, we use the types of particle density maps and histograms shown in Figure 1b to explain the two trends with increasing particle density highlighted in Figure 2c,d: (i) the shift to a higher frequency response at low-to-medium particle densities and (ii) the increase in low-frequency current at medium-to-high particle densities.

Interparticle Repulsion Increases the Effective Diffusion Rate and Reduces Effective Spatial Periodicity, Allowing for Higher Operating Frequencies

The transport process illustrated in Figure 1b requires the particles to reach the barriers between potential wells during the *spread* phase, so that, when the potential turns attractive again, they can be drawn to an adjacent spatial period. The spreading process for non-interacting particles relies on the interaction of the applied potential with each individual particle and on diffusion due to Brownian motion. Figure 3a, left, shows the spatial densities of either non-interacting or 512 interacting particles at four time-steps during a single oscillation, at the much higher oscillation frequency of f = 50 kHz (compared to 5 kHz for Figure 1b).

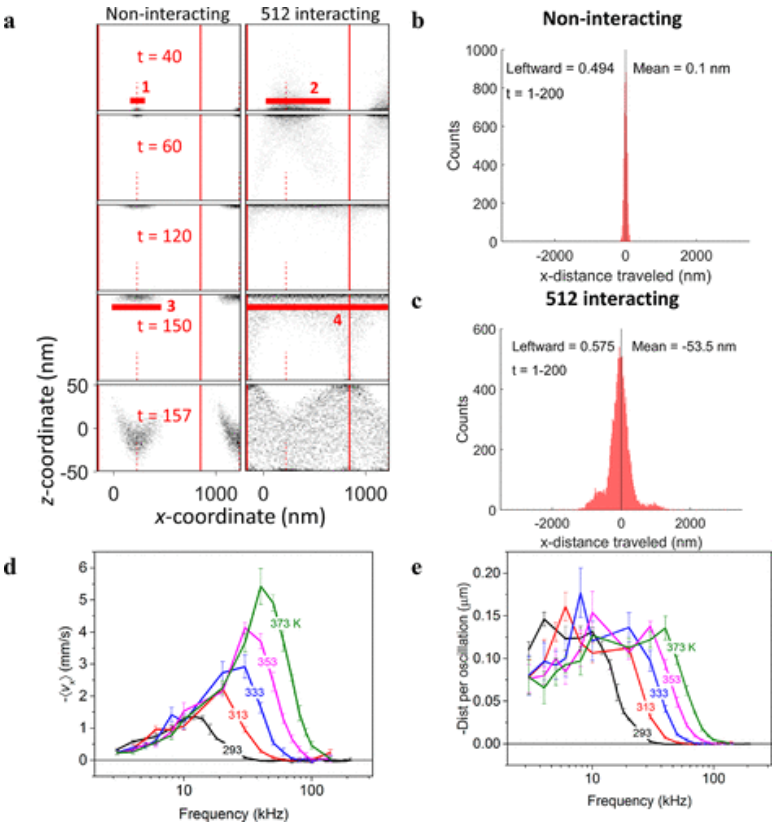

Figure 3. (**a**) Normalized density of non-interacting particles, and 512 interacting particles at specific time steps (indicated, of 200 per oscillation) during the simulation, focusing on one part of the simulation box, for $f = 50$

kHz. (**b**, **c**) Histograms of the distance traveled over an oscillation at $f = 50$ kHz by non-interacting (b) and 512 interacting particles (c); also indicated are the fraction of particles that traveled to the left and the mean travel distance of the ensemble. (a–c) Results from all analyzed oscillations and replicates. (**d**) Mean ensemble negative velocity as a function of oscillation frequency, for non-interacting particles at different temperatures (indicated); (**e**) the data in (d), divided by frequency, to give the distance traveled by the ensemble per oscillation. The values are the mean of four replicates, and the error bars are standard deviation of the mean.

In contrast with the transport achieved in Figure 1b, Figure 3a, left, shows that no ratcheting occurs for non-interacting particles at this high operating frequency; the particles merely return to their original well at the end of the cycle (Figure 3b). The reason for the lack of transport is that the time during which particles can spread is shorter than the characteristic time to traverse the distance between wells (solid lines) and barriers (dashed lines). The maximum spread of the particles is marked by the red block labeled "3" (at $t = 150$ out of 200 per oscillation). No particles reach the barrier, and so none cross to the adjacent well.

For interacting particles, as shown in Figure 3a, right, interparticle repulsion acts as a strong driving force to spread the particles along the top boundary—see the maximum spread of the particles, marked by the red block labeled "4" (at $t = 150$). Additionally, when the particles repel each other, they are less localized in the wells during the *trap* stage than are non-interacting particles (see blocks "1" and "2", at $t = 40$, Figure 3a). Some start their journey at the top boundary closer to the barrier and therefore need to cover a shorter distance to travel to the next well. In essence, interparticle repulsion shortens the effective periodicity of the potential for some of the particles, and so rather than having one distinct spatial periodicity in the ratchet, we now have a collection of different periodicities, based on the particles' positions in the wells. Each periodicity results in a different cutoff frequency for ratchet operation, so interparticle repulsion results in an overall broadening of the cutoff frequency to include higher operating frequencies than in the non-interacting case, Figure 2c. This mutual repulsion-aided motion also broadens the histogram of average distance moved by the particles in achieving ratcheting: compare Figure 1c with Figure 3c.

The increased spreading of particles along the top boundary due to interparticle repulsion is, in its consequences, equivalent to lowering the viscosity of the medium. To demonstrate this analogy, we increased the temperature of the medium (decreasing the viscosity) for a system with non-interacting particles. The cutoff frequency for ratchet operation indeed shifts to higher frequency with increasing temperatures (Figure 3d,e). Note that the turn-off of current with increasing frequency (for various temperatures) is quite sharp in the non-interacting particle case, whereas for interacting particles (Figure 2c), the decrease in transport efficiency with increasing frequency is more gradual, especially for higher particle densities. Similarly, compare the sharp peaks of the velocity in Figure 3d with the much wider peaks of Figure 2a.

A higher temperature also increases the intensity of Brownian forces, however simulations where we independently modulate the intensity of Brownian forces but keep the viscosity of the medium constant show that Brownian forces have little impact on the observed transport (Figure S9 of the Supporting Information) and so are not responsible for the data in Figure 3e. This result is not surprising, as in this specific transport mechanism, the particles are almost constantly driven, as opposed to the classic on/off ratchet, where particles diffuse freely for long periods.

At Higher Particle Densities, Transport Occurs over a Larger Fraction of the Oscillation Cycle

We now focus on the dependence of ratchet current on particle density in the low-frequency region (<10 kHz), Figure 2d. Initially, there is little change in distance traveled per oscillation with increasing particle density in this region; however, we observe a factor of 2 increase in transport at low driving frequencies between 128

and 512 particles per box. To help understand this increase, we plot in Figure 4a the ensemble means of several relevant parameters during a single oscillation of the potential, at $f = 5$ kHz (left) and 50 kHz (right). In the top panels we plot the mean *z*-position, which shows how the particles oscillate between the top and bottom boundaries; higher particle densities are not as strongly localized as lower particle densities, especially at the top boundary, where the field is weakest, because interparticle repulsion forces the particles to spread over a larger volume.

Figure 4

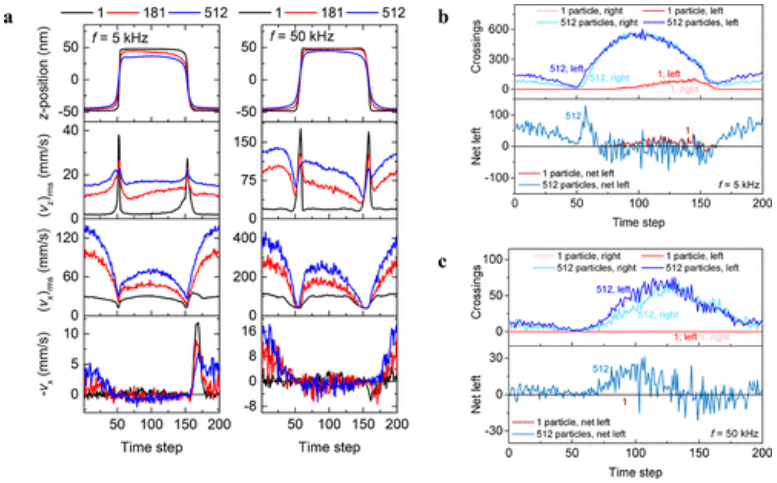

Figure 4. (**a**) Ensemble mean of the *z*-position, root-mean-square velocities in the *z*- and *x*-directions and velocity in the *x*-direction vs time step (of 200 per oscillation), averaged over all oscillations and replicates, for different particle counts (indicated), at $f = 5$ kHz (left) and $f = 50$ kHz (right). (**b**, **c**) Number of particles crossing the barrier between spatial periods, rightward and leftward, over the course of an oscillation (top), and the net crossing events leftward (bottom), for 1 and 512 interacting particles (indicated), at $f =$ (**b**) 5 and (**c**) 50 kHz.

In the middle two panels we plot the root-mean-square (rms) velocities in the *x*- and *z*-directions, which are measures of kinetic energy; with increasing particle density, rms velocities in both directions increase drastically. Notably, the dense, interacting particles remain highly mobile even during the *trap* stage at the bottom boundary. The high rms velocities also reflect the poor localization of interacting particles inside wells; rather, interacting particles accelerate toward the well, only to collide with other particles, be repelled, and accelerate again toward the well. Even at 5 kHz, the oscillation is too rapid to allow the particles to settle into equilibrium positions, maintaining an active nonequilibrium state.

In the bottom panels we plot the negative velocity of the particles in the *x*-direction (which serves as the observable for ratcheting); for non-interacting particles, transport (v_x) only occurs during a short fraction of the oscillation (see single peak around time step 170 in the black trace of Figure 4a, bottom left). In contrast, for higher densities of interacting particles, a longer fraction of each oscillation supports net transport, all while the particles are near the bottom boundary (time steps 1–50 and 150–200 in Figure 4a, bottom; see Figure S11 of the Supporting Information for other particle densities). This transport is correlated with high rms velocities of the particles even during the *trap* stage.

Figure 4b,c shows more explicitly how high kinetic energy and mobility of the particles during the *trap* stage, enabled by interparticle repulsion, translate to increased ratchet current at low frequencies. Here, we plot the number of border-crossing events, in the left or right directions, for different particle counts and oscillation frequencies. At $f = 5$ kHz (Figure 4b, top), non-interacting particles ("1") only cross the border between time steps 50 and 150 (*repel* and *spread* stages), when the particles are at the top boundary, in agreement with the

four-stage mechanism shown in Figure 1b. The net difference in crossings (Figure 4b, bottom) produces net transport. For 512 interacting particles, the same mechanism is seen, though crossings occur earlier in the cycle (closer to time step 50), due to the driving force produced by the interparticle repulsion, which helps the particles spread faster. Additionally, with 512 interacting particles, we also observe crossings while the particles are at the bottom boundary, time steps 1–50 and 150–200, with an even greater leftward bias. Even during the so-called "trap" stage, some interacting particles possess enough kinetic energy to escape their potential wells and freely explore the asymmetric potential surface, crossing the barriers between the wells. During their travel, they lose kinetic energy to friction and eventually settle in a new potential well. The asymmetric shape of the potential biases the particles' motion leftward, and the ratchet thus acts much like the temperature ratchet extensively studied in the literature.(1,35)

Crossings during the *trap* stage are seen to a much smaller degree at a faster driving frequency (Figure 4c), where presumably the oscillation is too fast to allow even the energetic interacting particles to meaningfully explore the space. The emergence of this repulsion-enabled mechanism for ratcheting at low frequencies and high particle densities is responsible for the enhancement of transport with increased density highlighted in Figure 2d and complements the previously discussed four-stage mechanism.

This new transport mechanism, where dense, energetic particles escape their traps and explore the asymmetric potential, gives rise to another result: at high densities, interacting particles can be transported across multiple spatial periods within one cycle of the potential. In Figure 5 we plot histograms of the distances traveled by individual particles over the course of an oscillation. Thirty-two interacting particles (Figure 5a) act like non-interacting particles at $f = 5$ kHz (Figure 1c); they might travel one period (1000 nm) to the left or right or simply return to their original positions. With increasing particle densities (Figure 5b,c and Figure S5 of the Supporting Information), growing fractions of particles travel two or even three periods in either direction in a single oscillation of the potential. The four-stage ratcheting mechanism we explained above (Figure 1b) does not include travel over multiple spatial periods. Energetic particles exploring the asymmetric potential, however, are not inherently limited to traversing a single spatial period, and their travel distances are determined by the duration of the *trap* stage and the rates of energy loss (to friction) and gain (from interparticle collisions and the potential). When the duration of the *trap* stage is reduced, at a driving frequency of $f = 50$ kHz, we only observe travel across single spatial periods, even for 512 interacting particles per box (Figure S6 of the Supporting Information). Particles traversing multiple spatial periods contribute proportionally to the mean distance traveled by the ensemble and also contribute to the observed increase in transport at low frequencies with increased particle density.

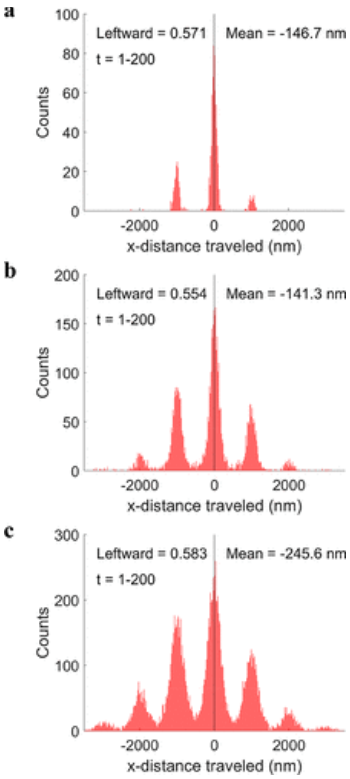

Figure 5. Histograms of the distance traveled by individual particles during a single oscillation, summed over all analyzed oscillations and over four replicates at $f = 5$ kHz, the fraction of particles that traveled to the left, and the mean travel distance of the ensemble over the oscillation, for (**a**) 32; (**b**) 181, and (**c**) 512 interacting particles.

Conclusions

In this work, we use classical simulations to explore the behavior of repulsively interacting particles in a 2D flashing ratchet. As the particle density increases, we find that the ratchet can be operated at higher and higher driving frequencies, producing greater transport velocities. The effective driving frequency is limited by the rate at which particles spread along a boundary in one stage of the ratcheting process, and interparticle repulsion provides an additional driving force to assist spreading. In addition, we find that high particle densities give rise to a new transport process at low driving frequencies. The new process results from weak localization of dense particles in wells during the *trap* stage, and it is distinct from the orderly four-stage process that dominates at low particle densities or high driving frequencies. Dense but weakly trapped particles occasionally obtain sufficient kinetic energy from interparticle collisions to escape their potential wells and explore the asymmetric potential surface. In their energetic state they may travel multiple spatial periods, a feat not possible in the four-stage ratcheting process.

These results have important implications for the design and operation of experimental ratchets. We have shown that the optimal operating frequency of the ratchet can be modified not only by changes to the spatial periodicity or inherent mobility of the device but also by modulating the particle density, the latter a much simpler modification. High density unlocks a new mode of ratcheting, which doubles the transport efficiency and provides transport over a much wider fraction of the cycle, smoothing the obtained current. Our results highlight the importance of characterizing device performance at different densities, as the differences in behavior as a function of density are both quantitative and qualitative. The insights into the substeps of the

ratcheting process, detailed in this work, enable the future tuning of the temporal driving and physical properties of ratchet devices to selectively address and modify rate-limiting steps.

Supporting Information

The Supporting Information is available free of charge on the ACS Publications website at DOI: 10.1021/acs.jpcc.9b00344.

Complete simulation details; viscosity plot; complete velocity and distance plots; additional histograms of the travel distances; mean ensemble velocity, *z*-position, rms *x*-velocity and *x*-velocity of non-interacting particles at different temperatures; ensemble *x*-velocity plots for each particle density for f = 5 and 50 kHz; velocity and distance versus frequency for non-interacting particles at different applied potential amplitudes (PDF)

References

1. Reimann, P. Brownian Motors: Noisy Transport Far from Equilibrium. *Phys. Rep.* 2002, *361*, 57– 265, DOI: 10.1016/S0370-1573(01)00081-3
2. Lau, B.; Kedem, O.; Schwabacher, J.; Kwasnieski, D.; Weiss, E. A. An Introduction to Ratchets in Chemistry and Biology. *Mater. Horiz.* 2017, *4*, 310– 318, DOI: 10.1039/C7MH00062F
3. Hänggi, P.; Marchesoni, F. Artificial Brownian Motors: Controlling Transport on the Nanoscale. *Rev. Mod. Phys.* 2009, *81*, 387– 442, DOI: 10.1103/RevModPhys.81.387
4. Astumian, R. D. Design Principles for Brownian Molecular Machines: How to Swim in Molasses and Walk in a Hurricane. *Phys. Chem. Chem. Phys.* 2007, *9*, 5067– 5083, DOI: 10.1039/b708995c
5. Hoffmann, P. M. How Molecular Motors Extract Order from Chaos (a Key Issues Review). *Rep. Prog. Phys.* 2016, *79*, 032601, DOI: 10.1088/0034-4885/79/3/032601
6. Chowdhury, D. Stochastic Mechano-Chemical Kinetics of Molecular Motors: A Multidisciplinary Enterprise from a Physicist's Perspective. *Phys. Rep.* 2013, *529*, 1– 197, DOI: 10.1016/j.physrep.2013.03.005
7. Astumian, R. D.; Bier, M. Fluctuation Driven Ratchets: Molecular Motors. *Phys. Rev. Lett.* 1994, *72*, 1766– 1769, DOI: 10.1103/PhysRevLett.72.1766
8. Müller, T.; Würtz, A.; Lorke, A.; Reuter, D.; Wieck, A. D. Wave-Form Sampling Using a Driven Electron Ratchet in a Two-Dimensional Electron System. *Appl. Phys. Lett.* 2005, *87*, 042104, DOI: 10.1063/1.2001740
9. Mikhnenko, O. V.; Collins, S. D.; Nguyen, T.-Q. Rectifying Electrical Noise with an Ionic-Organic Ratchet. *Adv. Mater.* 2015, *27*, 2007– 2012, DOI: 10.1002/adma.201404450
10. Bader, J. S.; Hammond, R. W.; Henck, S. A.; Deem, M. W.; McDermott, G. A.; Bustillo, J. M.; Simpson, J. W.; Mulhern, G. T.; Rothberg, J. M. DNA Transport by a Micromachined Brownian Ratchet Device. *Proc. Natl. Acad. Sci. U. S. A.* 1999, *96*, 13165– 13169, DOI: 10.1073/pnas.96.23.13165
11. Rousselet, J.; Salome, L.; Ajdari, A.; Prost, J. Directional Motion of Brownian Particles Induced by a Periodic Asymmetric Potential. *Nature* 1994, *370*, 446– 447, DOI: 10.1038/370446a0
12. Reimann, P. Current Reversal in a White Noise Driven Flashing Ratchet. *Phys. Rep.* 1997, *290*, 149– 155, DOI: 10.1016/S0370-1573(97)00064-1
13. Kostur, M.; Łuczka, J. Multiple Current Reversal in Brownian Ratchets. *Phys. Rev. E: Stat. Phys., Plasmas, Fluids, Relat. Interdiscip. Top.* 2001, *63*, 021101– 021101, DOI: 10.1103/PhysRevE.63.021101

14. Derenyi, I.; Ajdari, A. Collective Transport of Particles in a ”Flashing” Periodic Potential. *Phys. Rev. E: Stat. Phys., Plasmas, Fluids, Relat. Interdiscip. Top.* 1996, *54*, R5– R8, DOI: 10.1103/PhysRevE.54.R5
15. Conway, L.; Wood, D.; Tuzel, E.; Ross, J. L. Motor Transport of Self-Assembled Cargos in Crowded Environments. *Proc. Natl. Acad. Sci. U. S. A.* 2012, *109*, 20814– 20819, DOI: 10.1073/pnas.1209304109
16. Leduc, C.; Padberg-Gehle, K.; Varga, V.; Helbing, D.; Diez, S.; Howard, J. Molecular Crowding Creates Traffic Jams of Kinesin Motors on Microtubules. *Proc. Natl. Acad. Sci. U. S. A.* 2012, *109*, 6100– 6105, DOI: 10.1073/pnas.1107281109
17. Lipowsky, R.; Chai, Y.; Klumpp, S.; Liepelt, S.; Müller, M. J. I. Molecular Motor Traffic: From Biological Nanomachines to Macroscopic Transport. *Phys. A* 2006, *372*, 34– 51, DOI: 10.1016/j.physa.2006.05.019
18. Campàs, O.; Kafri, Y.; Zeldovich, K. B.; Casademunt, J.; Joanny, J. F. Collective Dynamics of Interacting Molecular Motors. *Phys. Rev. Lett.* 2006, *97*, 1– 4, DOI: 10.1103/PhysRevLett.97.038101
19. Lau, B.; Kedem, O.; Ratner, M. A.; Weiss, E. A. Identification of Two Mechanisms for Current Production in a Biharmonic Flashing Ratchet. *Phys. Rev. E: Stat. Phys., Plasmas, Fluids, Relat. Interdiscip. Top.* 2016, *93*, 062128, DOI: 10.1103/PhysRevE.93.062128
20. Kedem, O.; Lau, B.; Weiss, E. A. Mechanisms of Symmetry Breaking in a Multidimensional Flashing Particle Ratchet. *ACS Nano* 2017, *11*, 7148– 7155, DOI: 10.1021/acsnano.7b02995
21. Kedem, O.; Lau, B.; Ratner, M. A.; Weiss, E. A. A Light-Responsive Organic Flashing Electron Ratchet. *Proc. Natl. Acad. Sci. U. S. A.* 2017, *114*, 8698– 8703, DOI: 10.1073/pnas.1705973114
22. Kedem, O.; Lau, B.; Weiss, E. A. How to Drive a Flashing Electron Ratchet to Maximize Current. *Nano Lett.* 2017, *17*, 5848– 5854, DOI: 10.1021/acs.nanolett.7b03118
23. Aghababaie, Y.; Menon, G.; Plischke, M. Universal Properties of Interacting Brownian Motors. *Phys. Rev. E: Stat. Phys., Plasmas, Fluids, Relat. Interdiscip. Top.* 1999, *59*, 2578– 2586, DOI: 10.1103/PhysRevE.59.2578
24. Chacko, J.; Tripathy, G. Interacting Particles in Disordered Flashing Ratchets. *Indian J. Phys.* 2015, *89*, 981– 988, DOI: 10.1007/s12648-015-0660-5
25. Chakraborty, D.; Chaudhuri, D. Stochastic Ratcheting of Two-Dimensional Colloids: Directed Current and Dynamical Transitions. *Phys. Rev. E* 2015, *91*, 050301, DOI: 10.1103/PhysRevE.91.050301
26. Savel’ev, S.; Marchesoni, F.; Nori, F. Stochastic Transport of Interacting Particles in Periodically Driven Ratchets. *Phys. Rev. E* 2004, *70*, 061107– 061107, DOI: 10.1103/PhysRevE.70.061107
27. Einax, M.; Solomon, G. C.; Dieterich, W.; Nitzan, A. Unidirectional Hopping Transport of Interacting Particles on a Finite Chain. *J. Chem. Phys.* 2010, *133*, 054102– 054102, DOI: 10.1063/1.3463000
28. Cao, F.; Dinis, L.; Parrondo, J. M. R. Feedback Control in a Collective Flashing Ratchet. *Phys. Rev. Lett.* 2004, *93*, 040603, DOI: 10.1103/PhysRevLett.93.040603
29. Olson, C. J.; Reichhardt, C.; Jankó, B.; Nori, F. Collective Interaction-Driven Ratchet for Transporting Flux Quanta. *Phys. Rev. Lett.* 2001, *87*, 177002– 177002, DOI: 10.1103/PhysRevLett.87.177002
30. Stenhammar, J.; Wittkowski, R.; Marenduzzo, D.; Cates, M. E. Light-Induced Self-Assembly of Active Rectification Devices. *Sci. Adv.* 2016, *2*, e1501850 DOI: 10.1126/sciadv.1501850

31. Tierno, P.; Fischer, T. M. Excluded Volume Causes Integer and Fractional Plateaus in Colloidal Ratchet Currents. *Phys. Rev. Lett.* 2014, *112*, 1– 5, DOI: 10.1103/PhysRevLett.112.048302
32. Brown, A. I.; Sivak, D. A. Allocating Dissipation across a Molecular Machine Cycle to Maximize Flux. *Proc. Natl. Acad. Sci. U. S. A.* 2017, *114*, 11057– 11062, DOI: 10.1073/pnas.1707534114
33. Linke, H.; Downton, M. T.; Zuckermann, M. J. Performance Characteristics of Brownian Motors. *Chaos* 2005, *15*, 26111, DOI: 10.1063/1.1871432
34. Chung, J.; Hulbert, G. M. A Time Integration Algorithm for Structural Dynamics with Improved Numerical Dissipation: The Generalized-α Method. *J. Appl. Mech.* 1993, *60*, 371– 375, DOI: 10.1115/1.2900803
35. Reimann, P.; Bartussek, R.; Hänggi, P.; Häußler, R. Brownian Motors Driven by Temperature Oscillations. *Phys. Lett. A* 1996, *215*, 26– 31, DOI: 10.1016/0375-9601(96)00222-8